Computerized Detection of Pulmonary Embolism in Spiral CT Angiography Based on Volumetric Image Analysis

Yoshitaka Masutani*, Heber MacMahon, and Kunio Doi

***Abstract*—A fully automated method for computerized detection of pulmonary embolism in spiral computed tomography angiography was developed based on volumetric image analysis. The detection method is based on segmentation of pulmonary vessels to limit the search space, and analysis of several three-dimensional features inside segmented vessel volume. The features utilized are vascular size, local contrast based on mathematical morphology, degree of curvilinearity based on second derivatives, and geometric features such as volume and length. Detection results were obtained for 19 clinical data sets and the performance of the method was evaluated. Using the number and locations of thrombi diagnosed by radiologists as the gold standard, 100% sensitivity was achieved with 7.7 false positives per case, and 85% sensitivity was obtained with 2.6 false positives. For identification of all the positive cases as positive, i.e., detection of at least one thrombus per positive case, 1.9 false positives per case were obtained. These preliminary results suggest that the method has potential for fully automated detection of pulmonary embolism.**

***Index Terms*—Computer-aided diagnosis, pulmonary embolism, segmentation, volumetric image analysis.**

I. Introduction

DIAGNOSIS of pulmonary embolism is often described as being difficult for radiologists. In spiral computed tomography (CT) angiography (CTA), more than 100 images, sometimes including images obtained using multiplanar reconstruction, are viewed in each case for detection of thrombi in pulmonary arteries. Thrombi are frequently difficult to distinguish from false positives when only sectional images are used. In CTA images, thrombi are generally recognized as dark regions within enhanced pulmonary arteries in CTA images, as shown in Fig. 1. False positives with CT values resembling those of thrombi are mainly lymphoid tissue adjacent to pulmonary arteries, streak artifacts radiating from the superior vena cava, and partial volume artifacts at vascular bifurcations [1]–[3]. Knowledge of the thoracic vascular system, adjacent anatomical structures, and the imaging modality in use is, therefore, indispensable for accurate diagnosis.

We have previously reported several techniques that contribute to computerized detection of pulmonary embolism in spiral CTA, based on segmentation of pulmonary vessels and three-dimensional (3-D) image features [4], [5]. The present paper, we describe a computerized method detecting pulmonary embolism in spiral CTA based on volumetric image analysis, with reference to detection results in 19 clinical cases.

Manuscript received May 13, 2002; revised August 14, 2002. This work was supported by USPHS under Grant CA62625 and Grant CA64370. This work was based on the research project in the Kurt Rossmann Laboratories for Radiologic Image Research, Department of Radiology, University of Chicago, Chicago, IL, USA. K. Doi and H. MacMahon are shareholders of R2 Technology, Inc., Los Altos, CA. The Associate Editor responsible for coordinating the review of this paper and recommending its publication was N. Karssemeijer. *Asterisk indicates corresponding author*.

*Y. Masutani is with the Department of Radiology, the University of Tokyo Hospital, 7-3-1 Hongo Bunkyo-ku, Tokyo 113-8655, Japan.

H. MacMahon and K. Doi are with the Department of Radiology, the University of Tokyo Hospital, Tokyo 113-8655, Japan.

Digital Object Identifier 10.1109/TMI.2002.806586

II. Materials and Methods

A. Volume Data Acquisition in Spiral CT Angiography

The acquisition parameters for spiral CTA examinations at our institution include 3.0-mm collimation, 1.7 pitch, a 1.5-mm reconstruction interval, and a 3 cc/s injection rate for contrast agent. Imaging range extends from the top of the aortic arch to the diaphragm. Volume data sets in matrices of $512 \times 512 \times 60$–70 were interpolated using a linear method in ratios of 2.0–3.0 to yield isotropic volume data, which are relevant to volumetric image analysis. Finally, the data sets are reformatted into matrices of $512 \times 512 \times 150$–$250$ with a 0.6- to 0.7-mm voxel size.

B. Segmentation of Pulmonary Vessels

We segmented the pulmonary vessels to reduce the search space and eliminate false positives outside the vascular structures. We have reported on a segmentation technique for pulmonary vessels based on anatomical knowledge [6]. The segmentation result obtained with this method was used as an initial result in this study. In addition to the initial segmentation, further segmentation was performed for extraction of pulmonary vessels from main level to segmental and subsegmental levels of branches by removing contiguous cardiovascular structures such as cardiac ventricles and aorta.

Segmentation of pulmonary vessels in this method was performed in the following steps: preprocessing, segmentation of the major vascular structures, segmentation of peripheral vessels, and back-growing from the peripheral levels to major level of vascular structure.

In the first step, segmentation of the thoracic body and lungs, histogram acquisition, and removal of highly opacified regions (bone structures, etc.) are performed as preprocessing. Next, the major vascular structures, including the heart and the main branches of the pulmonary vessels, are segmented using

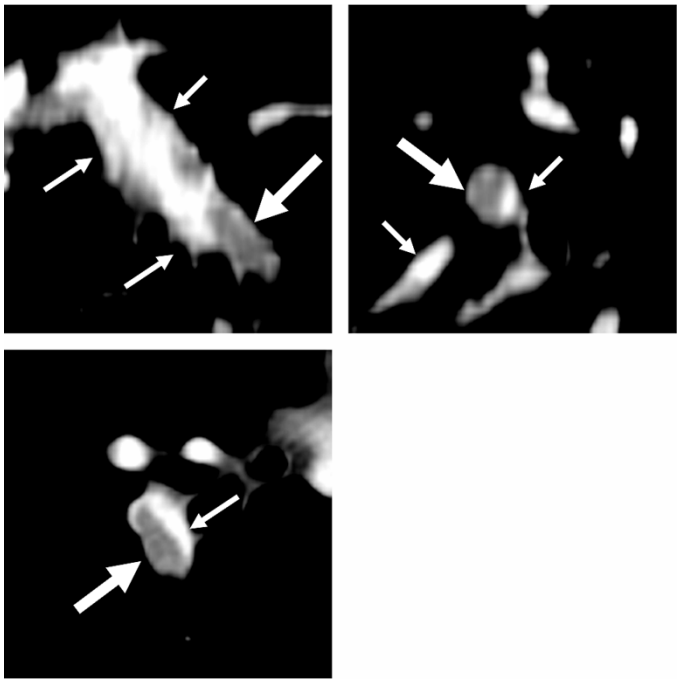

Fig. 1. Pulmonary embolism in spiral CT angiography. The CT values of thrombi (large arrows) are lower than those of the surrounding opacified regions of vessels (small arrows).

hysteresis thresholding [Fig. 2(a)] and connected-component analysis [Fig. 2(b)]. Hysteresis thresholding is a form of region (or volume)-growing techniques, in which seed regions are determined using another thresholding range narrower than the range for final region-growing. With the obtained major vascular structures utilized for a seed volume, peripheral vessels are segmented using region-growing [Fig. 2(c)]. The region-growing is limited to the inside of the lungs which have been segmented in the previous step. The result obtained up to this step is defined as an initial segmented volume. In the final step, back-growing is performed inside the initial segmented volume to fill the volume from the peripheral branches to the main branches. Peripheral vessels in the lungs [Fig. 2(d)] are defined as the seed volume for this back-growing. Back-growing is terminated at a pre-determined distance before the growth fronts reach the heart [Fig. 2(e)].

Fig. 2 shows an example of segmentation. Several segmentation parameters, such as thresholds, are determined adaptively and automatically, based on local histogram analyses inside the body [6]. In the volume of the final segmentation result [Fig. 2(f)], small defects and holes are filled using a binary closing operation of mathematical morphology with a spherical kernel (4-mm radius).

C. Analysis of 3-D Image Features Inside Segmented Vessels for Detection of Thrombi

After segmentation of pulmonary vessels, feature analysis for detection of thrombi is performed inside the segmented vessel volume. Thrombi are detected in two steps: 1) determination of initial candidates based only on the properties of voxels, and 2) determination of final candidates based on properties of the voxel group (connected component), such as volume and length.

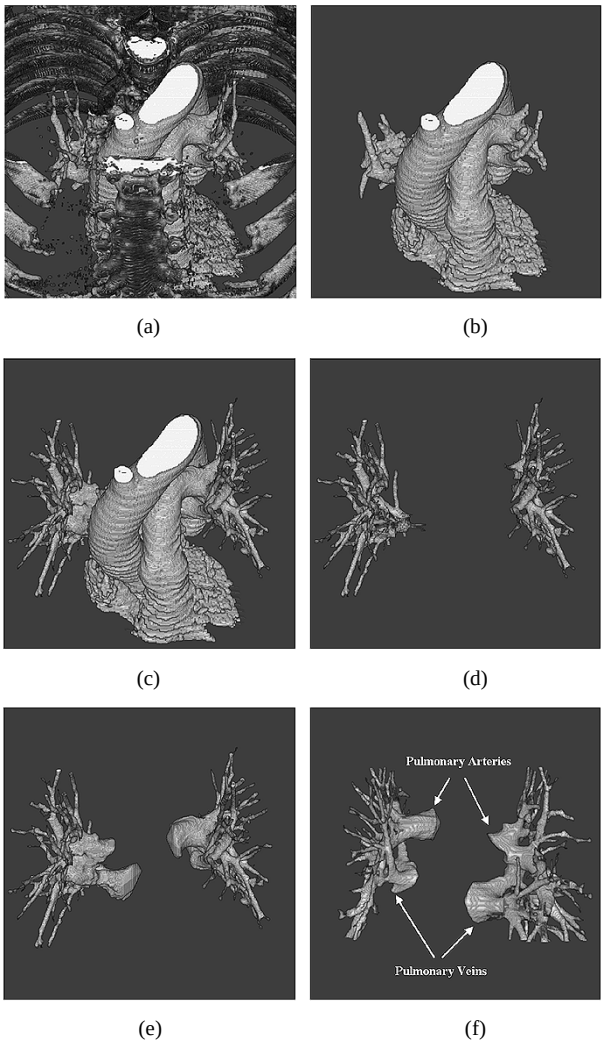

Fig. 2. Segmentation procedures. (a) Hysteresis thresholding result. (b) After connected-component analysis. (c) Region-growing in lungs. (d) Masking by lungs. (e) Back-growing to main branches. (f) Final segmentation result in posterior view. To limit the search for thrombi, pulmonary vessels from the main to the segmental and subsegmental levels of branches are segmented in several steps.

Basically, the former process involves the selection of voxels satisfying several conditions, and the latter involves the extraction of voxel groups after connected component analysis and determination of properties.

1) Analysis of Voxel Properties: CT values of thrombi are lower than those of the surrounding opacified regions of vessels. Conversely, CT values for opacified vessels are not uniform inside the segmented vascular volume. As we reported previously [5], voxels close to the vessel wall display lower CT values than distant voxels. This is largely attributable to the partial volume effect around the vessel wall. In addition, CT values of voxels depend on the vascular size. For such local variation of CT values inside segmented vessels, we defined the local contrast as an attribute of each voxel, based on grayscale morphology [7]. Local contrast is determined in two processes. One involves filtering of the original volume by grayscale closing only inside the segmented vascular shape. The other involves subtraction of the original volume from the filtered volume. The grayscale closing operation removes dark structures smaller

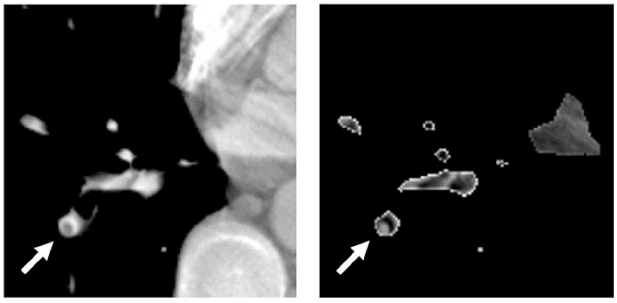

(a) (b)

Fig. 3. Local contrast. (a) Original data. (b) Local contrast in segmented vascular shape. A feature value, local contrast, is defined as an attribute of each voxel based on grayscale morphology.

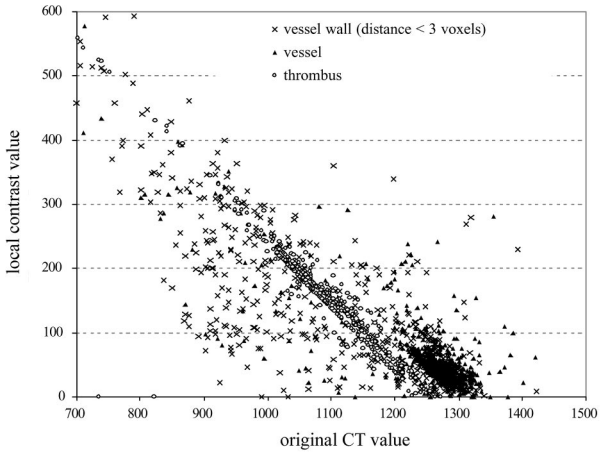

Fig. 4. Relationship between original CT values and local contrast values. Local contrast of thrombi exceeds that of opacified vessels, and that of the original CT values of thrombi is lower than that of opacified vessels. The vessel wall should be removed in distinguishing thrombi and opacified vessels to avoid a partial volume effect.

than the kernel employed, and subtraction of the original volume from the filtered volume extracts only the small, dark structures. The voxel value in the subtraction volume was defined as the local contrast at the location of the voxel, that is, the local contrast C_L of a voxel v is defined as

$$C_L(v) = V(v) - V_0(v) \tag{1}$$

where $V(v)$ denotes the original CT value of voxel v, and $V_0(v)$ is the CT value of a voxel v after filtering of the grayscale opening inside the segmented vascular shape. A spherical kernel (10-mm radius) was used for the opening operation in this study. An example of the volume data for local contrast obtained is shown in Fig. 3.

Fig. 4 shows the relationships between the original CT values and the local contrast values of three types of voxels: 1) voxels in thrombi defined by a radiologist; 2) in the vessel wall (three voxels in thickness), and; 3) in the remaining vascular volume. Voxels of the vessel wall are distributed in a broad range that overlaps the distributions of thrombi and opacified vessels. Therefore, removal of voxels around the vessel wall is indispensable for detection of thrombi using local contrast.

As an additional feature, we employed the second derivatives of the 3-D function of the volume data. As thrombi are formed predominantly in deep veins, a curvilinear structure is frequently evident. Multiscale analysis of second derivatives is widely used for enhancement or detection of curvilinear structures in two-dimensional and 3-D medical images [8], [9]. Three eigen values of a Hessian matrix, i.e., second derivatives in three orthogonal directions at a voxel, classify local patterns to which the voxel belongs. Based on the three values, a local pattern is classified to line-like (curvilinear), structure, plate-like, or blob-like structure. To quantify the degree of a structure being line-like, we defined the degree of curvilinearity of thrombi for each voxel as a feature value, based on a multiscale analysis to determine the second derivatives of voxels included in thrombi of various sizes.

First, second derivatives are computed in multiscale and in the three orthogonal directions that include the direction of the maximum second-derivative value. Multiscale analysis is performed in the scales from $\sigma_{\min}$ to $\sigma_{\max}$ with a pitch $\mathrm{d}\sigma$. As the structures of thrombi have intensities lower than those of the background level of enhanced vessels, the values of the second derivatives are basically positive in the direction perpendicular to the axis of the curvilinear structure. Our multiscale definition of the degree of curvilinearity of thrombi $D_{cl}(v, \sigma)$ is as follows:

$$D_{cl}(v) = \sum_{\sigma=\sigma_{\min}}^{\sigma_{\max}} sD_{cl}(v, \sigma) \times \mathrm{d}\sigma \tag{2}$$

where $sD_{cl}(v, \sigma)$ denotes the degree of curvilinearity of a voxel v in a single scale σ and $\mathrm{d}\sigma$ is a scale pitch. $sD_{cl}(v, \sigma)$ is defined as

$$sD_{cl}(v, \sigma) = \begin{cases} \lambda_2(v, \sigma) - \lambda_3(v, \sigma), & (\lambda_2(v, \sigma) > \lambda_3(v, \sigma) > 0) \\ \lambda_2(v, \sigma), & (\lambda_2(v, \sigma) > 0,\ \lambda_3(v, \sigma) < 0) \\ 0, & (\lambda_2(v, \sigma) < 0, \end{cases} \tag{3}$$

where λ_2 and λ_3 are the re-ordered values $(\lambda_1 > \lambda_2 > \lambda_3)$ of second derivatives at voxel v in three directions. In this study, we performed a multiscale analysis using scales $\sigma = 2.0$ to 4.0 in voxels and a scale pitch $\mathrm{d}\sigma = 0.2$. Basically, the difference between λ_2 and λ_3 was defined as the degree of curvilinearity so that the value would be low in cases the structure is sheet-like. If the second derivatives display negative values, the voxel has an intensity value higher than that of the background. In such cases, the degree of curvilinearity of thrombi is set as zero. Fig. 5 shows an example of the volume data obtained by calculating the degree of curvilinearity. Voxel values show the degree of curvilinearity in the lower row. It is clear that only the voxels that belong to curvilinear structures, i.e., thrombi, were enhanced while the others were suppressed. On the basis of the above two features, the initial candidate for thrombi is determined voxel by voxel. A voxel is included among the initial candidates if the original CT value of the voxel is within the range between -50 Hounsfield unit (HU) and 100 HU or the local contrast of the voxel exceeds 150 HU. Voxels on the vascular surface were removed to avoid partial volume effects. The thickness of the removed vascular wall was determined adaptively according to the vascular radius (Table I). Vascular size was determined by opening operations of mathematical morphology [4]. Finally, in

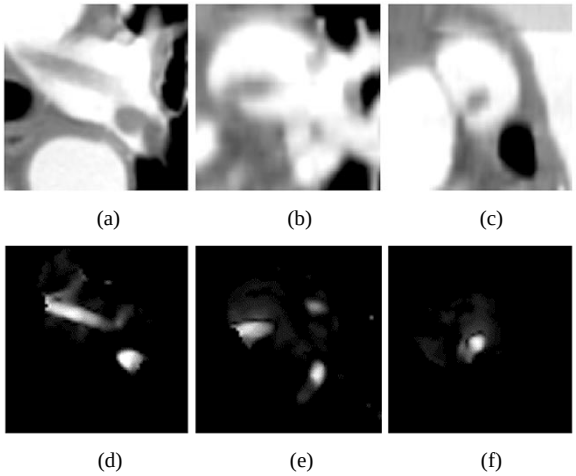

Fig. 5. Degree of curvilinearity. (a)–(c) Original data. (d)–(f) Degree of curvilinearity in segmented vascular shaped. A feature value, degree of curvilinearity of thrombi, is defined for each voxel, based on a multiscale analysis for determining the second derivatives of voxels.

TABLE I
THICKNESS OF REMOVED SURFACE VOXELS ADAPTIVELY DETERMINED FOR VASCULAR SIZE

Vascular radius (voxels)	Thickness of removed surface voxels
1 - 3	1
4 - 5	2
6 - 7	3
>= 8	4

addition to the candidates, voxels with a degree of curvilinearity in the range 40.0–80.0 were also added to the initial candidates for greater sensitivity of detection.

2) Analysis of Voxel Group Properties for Candidate Determination: After selection of the voxels as initial candidates, these voxels were converted into groups using connected-component analysis based on 26-neighbor connectivity. Candidates for thrombi were finally determined based on attributes of the voxel groups, which were volume (>10 mm^3), effective length (>10 mm), and mean local contrast (>60 HU, <300 HU) of the grouped voxels. The volume threshold was used to adjust sensitivity in the following test of the detection performance. To simplify the computation of the length of voxel groups, effective length was defined as the summation of width, height, and depth of the smallest box to cover the voxel group. Another feature related to the location of candidates, lung coverage, was used to eliminate false positives outside the lungs due to segmentation error. Lung coverage is the ratio of the number of voxels inside the lung to the number of voxels of the entire voxel group. Voxel groups with less than 0.75 of lung coverage were removed. Fig. 6 shows an overall flowchart of our computerized method.

III. RESULTS

A. Database for Detection Test

As a database for this study, we selected 19 (11 positive and 8 normal) cases from 30 clinical (20 positive and 10 normal) cases for validation of our computerized detection method, based on

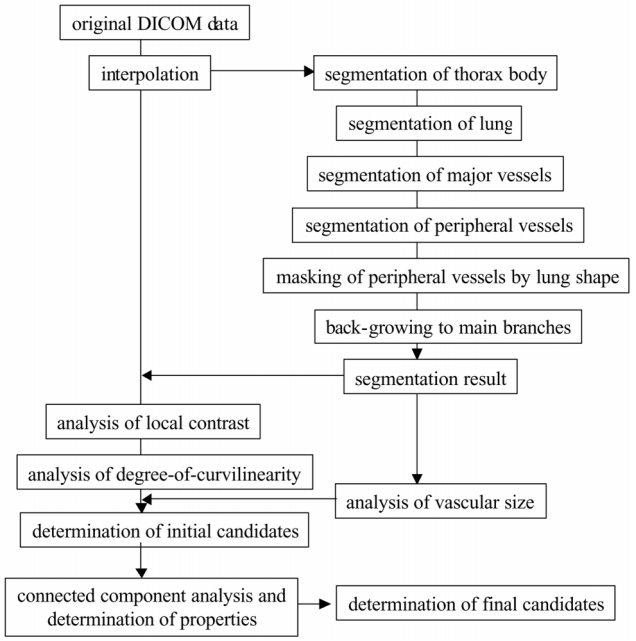

Fig. 6. Flowchart of overall detection scheme. After segmentation of pulmonary vessels, feature values are determined in the segmented vessels.

image quality of the data. We did not include data sets with strong motion artifacts, unsatisfactory vascular opacification or other diseases that would make the reliable definition of "truth" (i.e., gold standard of detection) difficult. To provide "truth" in each case, an experienced radiologist marked all locations of suspected thrombi, and voxel groups larger than 10.0 mm^3 in volume were selected for detection test in this study. Overall, 21 thrombi in the 11 positive cases were defined.

B. Detection Results

The detection of PE was performed in a fully automated manner from pre-processing of CTA data, through segmentation of anatomical structures, to the detection of thrombi. The time required for the entire detection from interpolation of data to determining the locations of candidates was 30–45 min, depending on the size of the data, using a PC workstation with 733-MHz Pentium III processor with 1-GB RAM.

To evaluate the performance of the method, we adjusted the detection sensitivity by changing the volume threshold of the final candidates of voxel groups and counted the average number of false positives per case. Using a 16 mm^3 volume threshold, the sensitivity was 100% with 7.7 false positives per case, and we obtained 85% sensitivity with 2.6 false positives per case using a 64 mm^3 volume threshold. Fig. 7 shows the FROC curve[10] for this detection test. We counted the number of false positives per case when identifying all positive cases as positive by adjusting the sensitivity. That is, at this setting of the volume threshold, we detected all of the largest thrombus in each case in this study. The number of false positives was 1.9 per case at a 95 mm^3 volume threshold.

Fig. 8 shows an example of the detection result for a thrombus in the left lower lobe. Several types of false positives were found in this study, such as lymphoid tissue, flow voids in both arteries and veins, soft tissue at a bifurcation, and averaging effects due

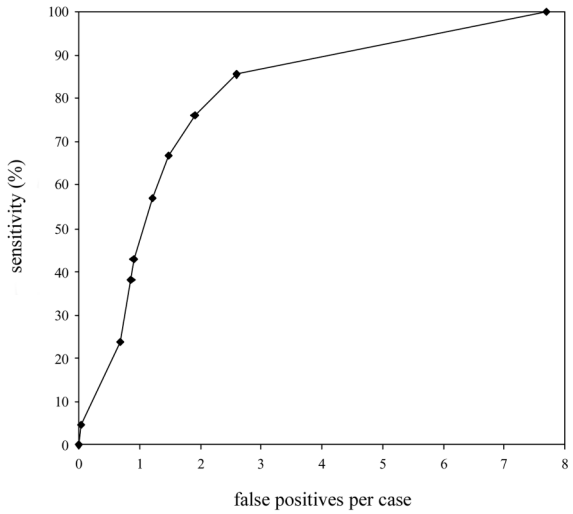

Fig. 7. FROC curve of detection results. Sensitivity of detection was adjusted by a threshold for candidate volume.

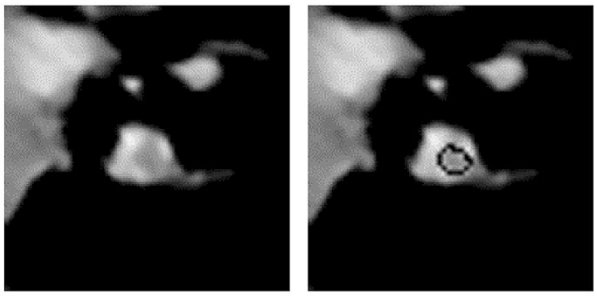

(a) (b)

Fig. 8. Example of detection result. (a) Original data. (b) Detection result (surrounded by a black line). Voxels close to vessel wall were not included based on removal of surface voxels on segmented vessel volume.

to the partial volume effect. These false positives are very similar to those obtained by radiologists [1]. Fig. 9 shows an example of false positive by the computerized method due to a flow void and soft tissue.

C. Display of Detection Results

For evaluation of this computerized method in clinical cases, a software system was developed to simultaneously display axial, coronal, and sagittal sections of a volume data set (Fig. 10). The software loads a detection result as a list of location coordinates, and shows three sectional views of planes that include the location, by selecting an item in the list. In addition to the three sectional views, volume rendering was utilized for visualizing segmented vessels and thrombi. Fig. 11(a)–(d) shows examples of detection results visualized using volume rendering [11]. Endoscopic views [12] of volume rendering were effective in showing how a thrombus occluded the vessels, as shown in Fig. 11(c).

IV. Discussion

As shown in Fig. 9, this computerized method displays high sensitivity for detecting low opacity regions inside segmented vessels, including flow void. False positives are attributable to soft tissues and flow voids in opacified vessels, which exhibit

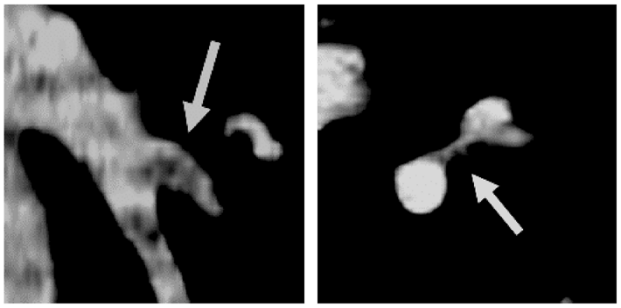

(a) (b)

Fig. 9. Example of false positives. (a) False positive due to flow void (arrow). (b) False positive due to soft tissue between adjacent vessels (arrow). As detection method has high sensitivity for detecting dark regions inside segmented vessels, false positives due to a flow void were obtained.

Fig. 10. Display system for detection result. By pointing a candidate on the right list, three sectional views of axial, coronal, and sagittal planes are displayed.

CT values and shapes similar to thrombi. A total of 143 false positives were obtained for the 19 cases (7.5 per case, on average) in the configuration for 100% sensitivity (Fig. 7). Among the false positives, 132 were related to soft tissues such as lymphoid tissue, which was included in the segmented vessel volume. Another six were based on segmentation errors of the vessel volume. In such cases, parts of bone structures were contiguous with the segmented volume. The remaining five false positives were due to flow void or noise inside vessels. In summary, 92% of the false positives were attributable to soft tissues such as lymphoid tissue surrounding vessels. One of the remaining problems in segmenting pulmonary vessels is the inclusion of such tissues. In a few cases with abnormally developed lymphoid tissues due to other diseases, more false positives were found than in other cases in our database. Removing all of these regions of soft tissues in the segmentation stage is difficult, because these regions have CT values very similar to those of thrombi. A feature value that would allow discrimination between soft tissues outside vessels and thrombi inside vessels would be valuable for this purpose. However, in a practical sense, these false positives due to soft tissue are not so critical, because they can usually be distinguished. Another problem is poor quality of original CT data. In this study, we excluded CT data sets obtained clinically, in which radiologists find difficulties for detecting thrombi and our computerized method failed in segmenting vessel structures. This is predominantly attributable to motion artifacts caused by patients. Sufficient consideration and checks for data quality

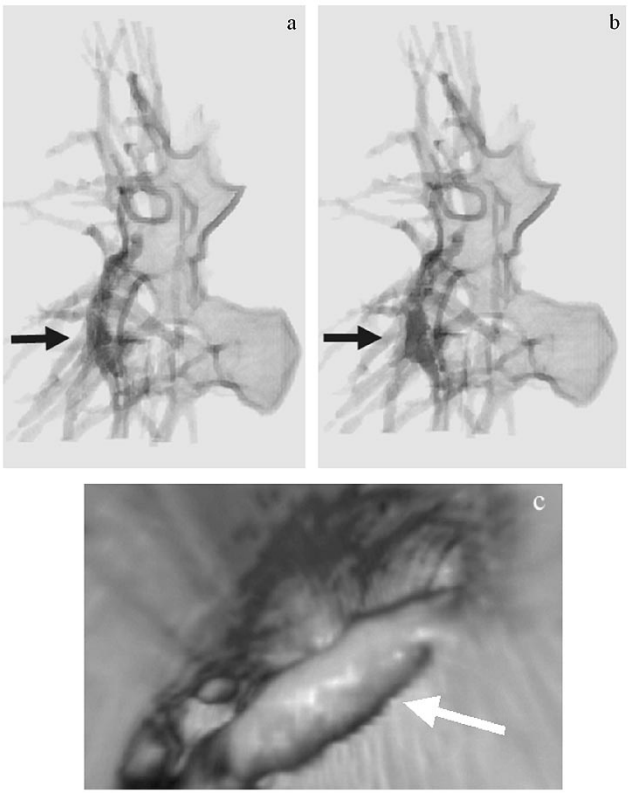

Fig. 11. Visualization of detection results under volume rendering. (a) Thrombus defined by radiologist in the left lower lobe pointed (arrow). (b) Detection result by computerized method pointed by (arrow). (c) Thrombus (arrow) visualized in endoscopic view. Volume rendering display of detection results including endoscopic views is effective for understanding the location of thrombi inside vessels and the state of occlusion.

are, therefore, requisite before applying our computerized method.

The percentages of the segmented volumes relative to total volume were less than 1%. The reduction of search space contributed to both efficiency of the detection process, and reduction of the number of false positives. However, the method depends strongly on the segmentation result for pulmonary vessels. If a blood vessel including a thrombus is not included in the segmentation result, the thrombus can never be detected. Although the segmentation procedure is a preprocessing step for detection of thrombi, this procedure should have high sensitivity in order to include as many vascular branches as possible. We adjusted this sensitivity to segment vessels larger than about 2 mm in diameter, by changing the lower threshold used in region-growing for segmentation of peripheral vessels [6].

Another segmentation issue involves contact between pulmonary arteries and pulmonary veins at the main branch level. We segmented both pulmonary arteries and veins in this method. As some false positives were identified in the pulmonary veins, further separation of arteries and veins seems likely to reduce false positives. Generally, the main branches of the pulmonary vessels at the right hilum are in intimate contact. The edges of the vessel walls are often unclear due to motion artifacts caused by the heart and blurring effects caused by interpolation in the axial direction. Consequently, the main branches of arteries and veins were segmented as a connected object.

We have analyzed another feature for detection of thrombi, based on vascular section properties. This method based on tree-structured information on vascular sections [13] displayed a high potential for detecting complete or nearly complete vascular occlusion by emboli, although high-quality data is required for analysis of bifurcation structures. Recent developments in multidetector CT are expected to greatly contribute to overcoming this obstacle by improving resolution in the Z direction, and by reducing data acquisition time.

The purpose of CTA examination is to judge whether an examined patient has thrombi in the pulmonary arteries, as treatment of pulmonary embolism is based on infusion of drugs into the entire vascular system. In this sense, detection of all thrombi in a patient is not strictly necessary. Although determining the best detection parameters for practical use is a difficult task, reasonable options can be found based on a sensitivity control using the FROC curve. For example, we obtained approximately six false positives to keep the detection sensitivity above 90%. Further investigation should be performed to determine the optimal configuration and improve detection performance.

V. Conclusion

We developed a new computerized method for detecting pulmonary embolism in spiral CTA, based on volumetric image analysis. On the basis of segmentation of pulmonary vessels, several 3-D features were analyzed for detection of thrombi, including local contrast and degree of curvilinearity. Detection results were obtained for 19 clinical data sets, and the performance was 7.7 false positives per case at 100% sensitivity, and 2.6 at 85%, to detect the all thrombi as defined by a radiologist. Conversely, 1.9 false positives per case were found by adjusting detection parameters to correctly identify all positive cases. Our preliminary results show that this method has potential for fully automated detection of pulmonary embolism.

Acknowledgment

The authors would like to thank all the members of the Rossmann Laboratories for their valuable discussions and encouraging advice. The software used in this study includes several software modules that were developed by Y. Masutani, Ph.D. at the University of Tokyo, Japan, and at the University of Hamburg, Germany. The authors would also like to thank Prof. T. Dohi of the University of Tokyo and Prof. K.-H. Hoehne of the University of Hamburg for their permission to use these software modules.

References

[1] M. Remy-Jardin, Ed., *Spiral CT of the Chest (Medical Radiology)*. Berlin, Germany: Springer-Verlag, 1996.

[2] C. Beigelman, C. Chartrand-Lefebvre, N. Howarth, and P. Grenier, "Pitfalls in diagnosis of pulmonary embolism with helical CT angiography," *Amer. J. Radiol.*, vol. 171, pp. 579–585, Sept. 1998.

[3] R. M. Summers, "Morphometric methods for virtual endoscopy reconstructions," in *Handbook of Medical Imaging: Processing and Analysis*, I. N. Bankman, Ed. New York: Academic, 2000, ch. 45, pp. 747–755.

[4] Y. Masutani, H. MacMahon, and K. Doi, "Computer-assisted detection of pulmonary embolism," *Proc. SPIE (Medical Imaging 2000)*, pt. II, vol. 3979, pp. 944–950.

[5] ——, "Computerized detection of pulmonary embolism in spiral CT angiography: A segmentation-based approach using 3D image analysis and anatomical knowledge," in *Proc. Computer-Assisted Radiology and Surgery*, H. U. Lemke, M. W. Vannier, K. Inamura, A. G. Farman, and K. Doi, Eds., 2000, pp. 779–784.

[6] ——, "Automated segmentation of the pulmonary vascular tree in spiral CT angiography for computerized detection of pulmonary embolism," in *Med. Phys. 26 (AAPM Annu. Meeting Issue)*, 1999, p. 1101.

[7] S. R. Sternberg, "Grayscale morphology," *CVGIP*, vol. 35, no. 3, pp. 333–355, 1986.

[8] Y. Sato *et al.*, "Three-dimensional multi-scale line filter for segmentation and visualization of curvilinear structures in medical images," *Med. Image Anal.*, vol. 2, pp. 143–168, 1998.

[9] C. Lorenz, I.-C. Carlsen, T. M. Buzug, C. Fassnacht, and J. Weese, "Multi-scale line segmentation with automatic estimation of width, contrast and tangential direction in 2D and 3D medical images," in *Proc. CVRMed-MRCAS'97*, 1997, pp. 233–242.

[10] C. E. Metz, "Basic principles of ROC analysis," *Seminars Nucl. Med.*, vol. 8, pp. 283–298, 1978.

[11] M. Levoy, "Display of surfaces from volume data," *IEEE Comput. Graphics Applicat.*, vol. 8, pp. 29–37, 1988.

[12] M. E. Ladd *et al.*, "Virtual MR angioscopy of pulmonary artery tree," *JCAT*, vol. 20, pp. 782–785, 1996.

[13] Y. Masutani, T. Schiemann, and K. H. Hoehne, "Vascular shape segmentation and structure extraction using a shape-based region-growing model," in *Proc. MICCAI '98*, 1998, pp. 1242–1249.